Time-Mean Response over the Tropical Pacific to Increased CO$_2$ in a Coupled Ocean–Atmosphere Model

THOMAS R. KNUTSON AND SYUKURO MANABE

Geophysical Fluid Dynamics Laboratory/NOAA, Princeton, New Jersey

ABSTRACT

The time-mean response over the tropical Pacific region to a quadrupling of CO$_2$ is investigated using a global coupled ocean–atmosphere general circulation model. Tropical Pacific sea surface temperatures (SSTs) rise by about 4°–5°C. The zonal SST *gradient* along the equator decreases by about 20%, although it takes about one century (with CO$_2$ increasing at 1% per year compounded) for this change to become clearly evident in the model. Over the central equatorial Pacific, the decreased SST gradient is accompanied by similar decreases in the easterly wind stress and westward ocean surface currents and by a local maximum in precipitation increase.

Over the entire rising branch region of the Walker circulation, precipitation is enhanced by 15%, but the time-mean upward motion *decreases* slightly in intensity. The failure of the zonal overturning atmospheric circulation to intensify with a quadrupling of CO$_2$ is surprising in light of the increased time-mean condensation heating over the "warm pool" region. Three aspects of the model response are important for interpreting this result. 1) The time-mean radiative cooling of the upper troposphere is enhanced, due to both the pronounced upper-tropospheric warming and to the large fractional increase of upper-tropospheric water vapor. 2) The dynamical cooling term, $-\bar{\omega}\partial\bar{\theta}/\partial p$, is enhanced due to increased time-mean static stability ($-\partial\bar{\theta}/\partial p$). This is an effect of moist convection, which keeps the lapse rate close to the moist adiabatic rate, thereby making $-\partial\bar{\theta}/\partial p$ larger in a warmer climate. The enhanced radiative cooling and increased static stability allow for the enhanced time-mean heating by moist convection and condensation to be balanced without stronger time-mean upward motions. 3) The weaker surface zonal winds and wind stress in the equatorial Pacific are consistent with the reduced zonal SST gradient. The SST gradient is damped by the west–east differential in evaporative surface cooling (with greater evaporative cooling in the west than in the east). This evaporative damping increases with increasing temperature, owing to the temperature dependence of saturation mixing ratios, which leads to a reduction in the SST gradient in the warmer climate.

1. Introduction

Using a global coupled ocean–atmosphere general circulation model (GCM), the time-mean response over the tropical Pacific region to increased CO$_2$ is investigated. The response in this region is of particular interest for several reasons. For example, the present-day tropical Pacific climate is notable for its pronounced zonal asymmetry, with atmospheric rising motion and frequent tropical convective activity occurring over the western Pacific warm pool and sinking motion and less frequent convection over the cooler eastern Pacific. Carbon dioxide-induced changes in this zonal asymmetry could have dramatic impacts on the distribution of large-scale atmospheric heating, as occurs during El Niño–Southern Oscillation events, which in turn could substantially affect the large-scale extratropical circulation. As another example, since the western tropical Pacific has the warmest open-ocean surface temperatures found on earth, a significant CO$_2$-induced warming would result in warm SST conditions unlike any found in the earth's present climate; Emanuel (1987) has suggested that such a warming could lead to an increased maximum potential intensity for tropical cyclones.

In the present study, the focus is on changes in the *time-mean* heating by convection and condensation and its effect on the time-mean atmospheric circulation over the tropical Pacific. In a related study (Knutson and Manabe 1994) we have shown that the ENSO-like SST fluctuations in our coupled ocean–atmosphere model *decrease* slightly in intensity as a result of CO$_2$-induced warming.

A major element of the study is an analysis of the model's atmospheric heat and moisture budgets. These results are used to help interpret the relationship between CO$_2$-induced changes in heat released by condensation and the atmospheric circulation. The results can be compared to previous studies of the heat and moisture budgets using GCMs (Mitchell and Ingram 1992; Del Genio et al. 1991) or observations (Cornejo-Garrido and Stone 1977). Although we will not focus on the role of interactive cloud in the tropical response to increased CO$_2$, Wetherald and Manabe (1988) have

Corresponding author address: Thomas R. Knutson, NOAA/ GDFL, P.O. Box 308, Princeton, NJ 08542.

analyzed these cloud effects using a version of the GFDL climate model similar to that used for our study.

This report is organized as follows. In section 2, descriptions of the model and experiments are given. Section 3 contains a description of the response of tropical SSTs, precipitation, and circulation to increased CO_2. In sections 4, 5, and 6 the balances of atmospheric heat, moisture, and surface energy are examined. In section 7 the main points of the study are discussed and summarized, including a comparison with the response of the model's ENSO-like phenomena. Appendix A contains a detailed description of the model's temperature and moisture tendency equations. In appendix B, the resolution dependence of certain results is explored using an atmospheric model with twice the horizontal resolution of that used for the main study.

2. Description of model and experiments

The model used for the main analysis is a GFDL global coupled ocean–atmosphere general circulation model (GCM). Briefly, the atmospheric component is a global nine-level spectral GCM (Gordon and Stern 1982) with the horizontal distribution of variables represented in both spectral (rhomboidal truncation at zonal wavenumber 15) and gridpoint (7.5° longitude by 4.5° latitude computational grid) domains. The ocean component is a 12-level gridpoint GCM with horizontal resolution of 3.75° longitude by 4.5° latitude. The coupled model's parameterizations include moist convective adjustment (Manabe et al. 1965), predicted clouds (Wetherald and Manabe 1988), and seasonally (but not diurnally) varying solar insolation. To prevent spurious climate drift from a realistic initial condition the surface fluxes of heat and water imposed upon the oceanic component of the model are adjusted by an amount that varies geographically and seasonally (Manabe and Stouffer 1994). The adjustment, however, has no interannual variation and, therefore, is independent of the anomalies of SST and salinity. Thus, the adjustments neither directly amplify nor directly damp the anomalies. The atmosphere and ocean components, coupling framework, and basic experiments are described more fully in Manabe et al. (1990; 1991), Manabe and Stouffer (1993; 1994), and references therein.

The CO_2 perturbation experiment analyzed in this study is described in Manabe and Stouffer (1993, 1994). In the experiment, CO_2 increases at 1% yr^{-1} compounded to four times its initial level (after 140 years), then remains constant at the 4 × CO_2 level for the final 360 years of a 500-year integration. The eventual quadrupling of atmospheric CO_2 is assumed referring to the study of Walker and Kasting (1992). Their study suggests that draconian measures would probably be required to prevent an eventual quadrupling of atmospheric CO_2. Regardless of whether a quadrupling of CO_2 eventually occurs, the 4 × CO_2 experiment facilitates the investigation of the tropical response to increased CO_2 by enhancing the signal to noise ratio.

In the present report, the term "4 × CO_2 experiment" is used to refer to years 401–500 of the CO_2 perturbation experiment, although the climate had not yet fully "equilibrated" to the 4 × CO_2 radiative perturbation, partly due to the large thermal inertia of the deep ocean. The term "control experiment" is used to refer to the first 100 years of a constant 1 × CO_2 experiment, which serves as a comparison for the 4 × CO_2 experiment. Owing to the large climate perturbation with 4 × CO_2 and the 100-year averaging interval, our results are very similar if other 100-year segments of the control run are used as a comparison.

The high-resolution model used for the sensitivity analysis (appendix B) has twice the horizontal resolution, 14 vertical levels, and is coupled with a mixed layer rather than a general circulation model of the oceans. Other differences between the high- and low-resolution models are discussed in appendix B. Although the high-resolution simulation appears to be better than that of the low-resolution model for certain fields (e.g., tropical precipitation and sea level pressure), the emphasis in the present study is on results from the low-resolution model. This is because the coupled low-resolution simulation alone incorporates important ocean dynamical effects in the CO_2-induced response. Nevertheless, the high-resolution simulation is a very useful complement to the low-resolution results because it provides an initial assessment of the impact on our conclusions of using a relatively low-resolution (R15) atmospheric model.

3. SST, precipitation, and circulation response

In the 4 × CO_2 experiment, the tropical SSTs increase fairly uniformly by about 4.6°C (Fig. 1). Surface air temperature over tropical land (not shown) increases by about 6°C on average. The general *pattern* of the SST field in the 4 × CO_2 experiment, including locations of maxima and minima, remains similar to that of the control run. However, close inspection of Fig. 1c indicates that the zonal SST gradient in the equatorial Pacific is reduced by about 20%, with a warming of up to 5.3°C in the eastern equatorial Pacific, compared with about 4.2°C in the western Pacific.

As a result of the SST warming in the 4 × CO_2 experiment, the regions with annual-mean SST > 28°C expand eastward to cover almost the entire tropical ocean domain and expand poleward to about 30° latitude over much of the oceans (Fig. 1b). Observations of the present-day climate (e.g., Graham and Barnett 1987) indicate that large-scale deep tropical convection occurs in association with SSTs in excess of 27.5°C. However, as shown in Figs. 2a,b, the basic pattern of tropical precipitation in the 4 × CO_2 experiment is
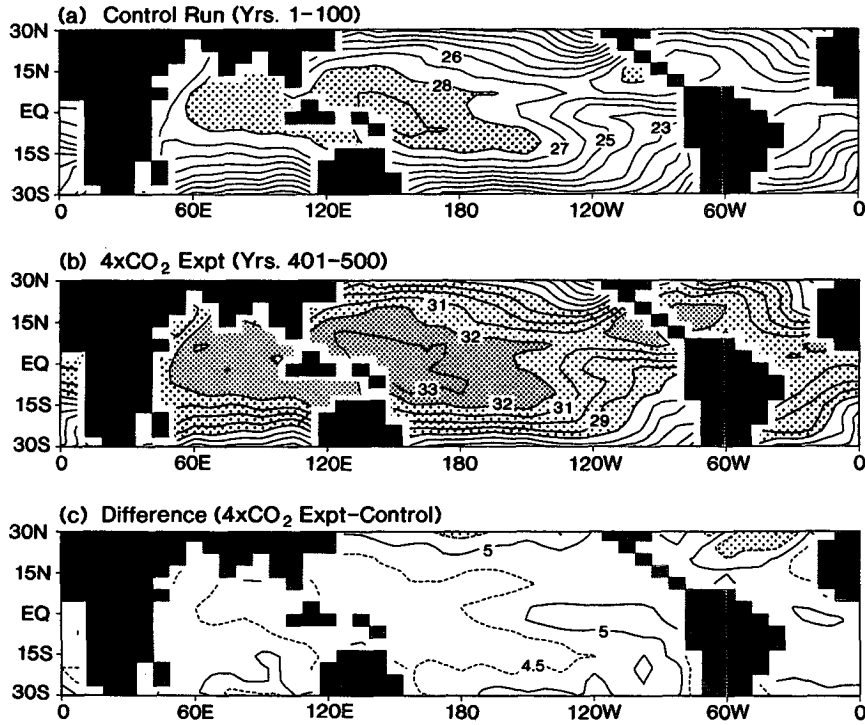
FIG. 1. Annual mean sea surface temperature for the (a) control run (years 1–100), (b) 4 × CO_2 experiment (years 401–500), and (c) difference (b − a). Contour intervals: 1°C (a, b) and 0.5°C (c).
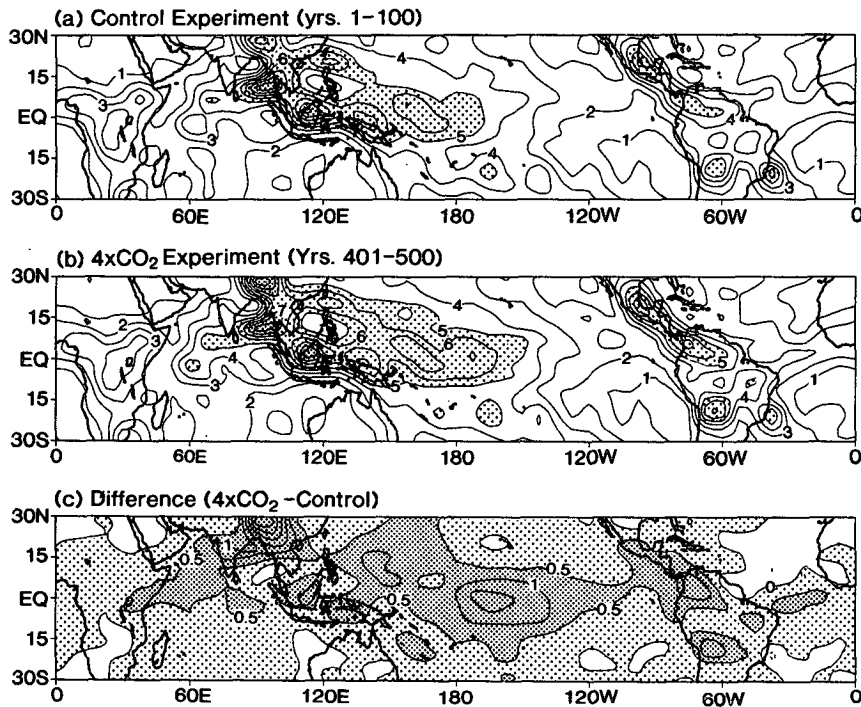

FIG. 2. Annual mean precipitation for the (a) control run (years 1–100), (b) 4 × CO_2 experiment (years 401–500), and (c) difference (b − a). Contour intervals: (a, b) 1.0 mm day^{-1} and (c) 0.5 mm day^{-1}. Values greater than 5 mm day^{-1} (a), (b) or 0.0 (c) have light shading. In (c) values exceeding 0.5 mm day^{-1} have dark shading.

very similar to that of the control experiment, with only a slight expansion of the region with precipitation of 5 mm day^{-1} or more, despite the dramatic expansion of the region with SST > 28°C. In fact, 32°–33°C, rather than 28°C, appears to delineate the primary tropical precipitation regions in the 4 × CO_2 experiment. These results suggest that 28°C is not a universally applicable "threshold temperature" for determining the primary tropical convection regions but that these regions will tend to be located in tropical areas where SSTs are *higher than in surrounding regions*. Neelin and Held (1987), arrived at a similar conclusion based upon analysis of the moist static energy budget.

Although the pattern of tropical rainfall remains similar overall, most tropical regions have some increase in rainfall in the 4 × CO_2 experiment (denoted by the shaded regions in Fig. 2c). The areas of maximum absolute increase are over the central equatorial Pacific (consistent with the local maximum in SST warming in the central and eastern Pacific) and on the southern upslope of the model's Tibetan Plateau (a monsoon feature which will be the subject of a future analysis using a higher-resolution version of the model). Rainfall also increases by more than 1 mm day^{-1} over parts of the western tropical Pacific and South America. Although the CO_2-induced *fractional* increases in zonal mean tropical precipitation are not as large as those in high latitudes (Manabe et al. 1991), about one-half of the globally integrated precipitation increase occurs within 30° of the equator. The zonal mean increases in precipitation migrate north and south in the model, following the seasonal march of the tropical "wet" season.

The vertically integrated water vapor in the Tropics increases by a much greater percentage (+48%) than either precipitation (+13%) or evaporation (+15%). This feature was also noted by Randall et al. (1992) in the global response of several other GCMs to a uniform warming. The much larger fractional increase in water vapor compared to precipitation, which is also the case for the model global means (+54% vs +14%), implies a longer average atmospheric residence time for water vapor. Thus, this change could have implications for atmospheric chemistry that are well beyond the scope of the present study. We will return to the topic of water vapor increases versus precipitation increases in section 6.

In Fig. 3 are climatologies of zonal wind and vertical velocity from the 4 × CO_2 and control experiments. The climatologies from the control experiment (Figs. 3a,d) depict well-known features of the tropical Pacific atmospheric circulation, including pronounced rising motion over Indonesia and western Pacific, subsidence in the eastern Pacific, and easterly winds near the surface over the central and eastern Pacific. There are some notable biases relative to observed climatologies, including a westerly bias in the tropical upper troposphere, as noted by Rosen and Gutowski (1992). The

zonal mean, seasonal mean vertical velocities in the Tropics are about 30% weaker than Oort's (1983) estimates for the real world. However, the first-order structure of the observed large-scale tropical circulation is reasonably well-simulated with the low-resolution model.

Figure 3 illustrates that the basic structure of the large-scale tropical circulation remains similar in the 4 × CO_2 experiment to that in the control experiment, although many of the features are slightly less intense in the 4 × CO_2 experiment (particularly in the lower and midtroposphere). Of particular note is the *decreased* intensity of time-mean rising motion over the Indian Ocean, Indonesia, and the western Pacific (Fig. 3f) despite the *increased* precipitation noted earlier. A relatively small area of enhanced time-mean rising motion occurs just east of the date line (Fig. 3f) where a local maximum in precipitation increase occurs (Fig. 2c). Near-surface zonal winds over the central Pacific and the time-mean subsidence over the eastern Pacific are also slightly weaker with 4 × CO_2. The model's Hadley circulation (not shown) exhibits a slight CO_2-induced decrease in intensity through most of the lower and middle troposphere along with a slight upward expansion of the circulation cells in the upper troposphere. In light of the enhanced condensation heating, the lack of intensification of the time-mean rising motion in the model is surprising and will be investigated in greater detail in section 4.

The model's annual-mean surface wind stress and ocean surface-layer current climatologies are shown in Figs. 4 and 5. As in the annual mean simulation of Lau et al. (1992) the model's surface wind stress is about 30%–50% weaker than observed (Hellerman and Rosenstein 1983). The meridional surface wind convergence in the northeast tropical Pacific is also notably weaker than observed. However, the first-order structure of the observed surface wind stress climatology is reasonably well simulated in the model. The model's westward equatorial ocean current, as in the study of Lau et al. (1992), is roughly a factor of 2 weaker than observed (Peixoto and Oort 1992), and the north equatorial countercurrent is not reproduced. Philander et al. (1992) have shown that these ocean simulation deficiencies can be greatly reduced using an ocean model with much higher resolution. In addition, we have found that the tropical Pacific surface easterlies and meridional convergence in the northeast Pacific ITCZ region are substantially stronger in a higher-resolution version of the atmospheric model (described in appendix B).

In response to a quadrupling of CO_2, the surface easterly wind stress over the equatorial Pacific (2°N–2°S, 172.5°E–112.5°W) weakens by 15% relative to the control experiment (Fig. 4c); the surface easterly winds decrease by 12%. The large-scale surface pressure gradient (as measured by the surface pressure for the region 2°N–2°S, 142.5°W–82.5°W minus that for
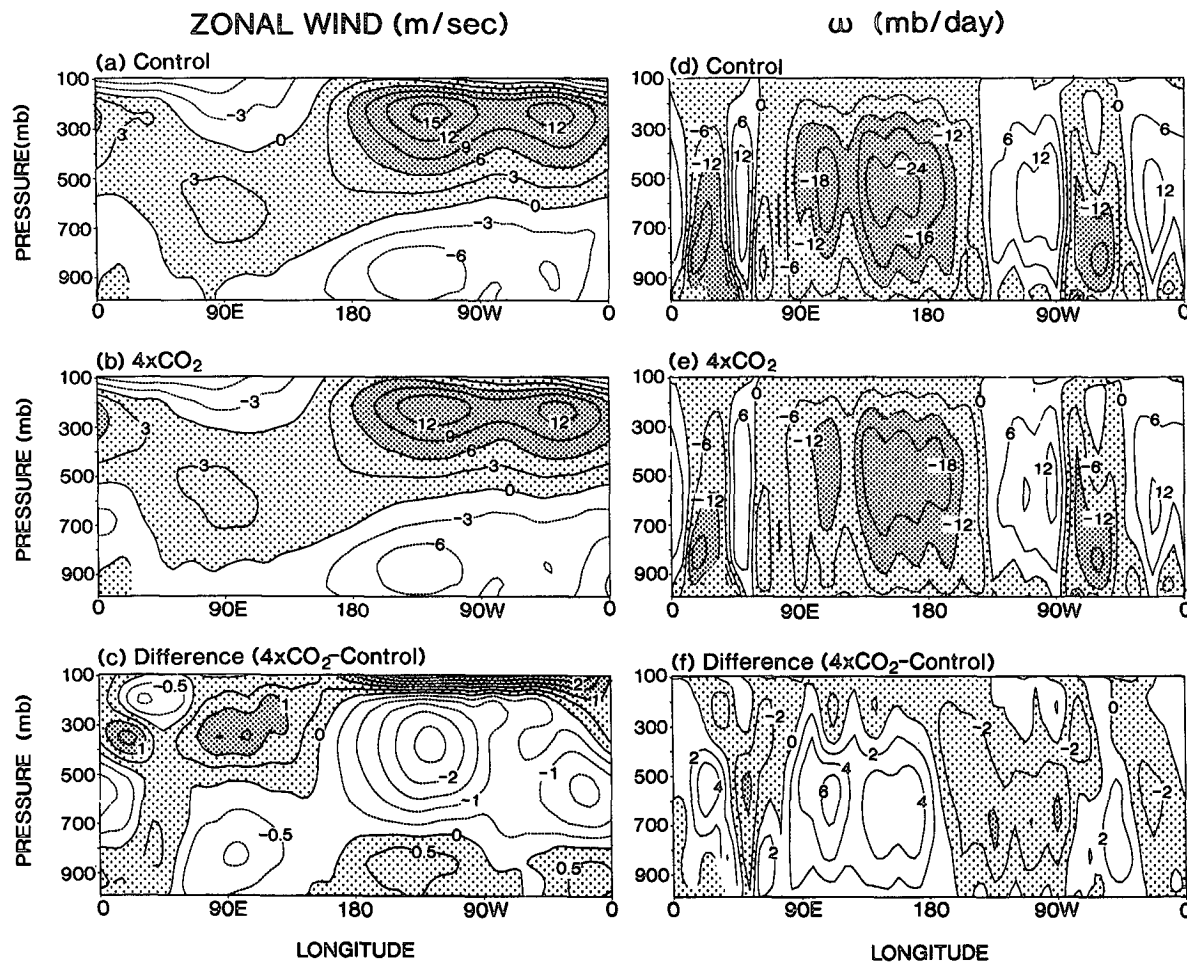
ZONAL WIND (m/sec)

ω (mb/day)

FIG. 3. Longitude vs pressure profiles of (a–c) zonal wind, with positive values shaded; and (d–f) vertical pressure velocity, ω = dp/dt, with negative values shaded. Based on annual mean data, averaged 11°N to 11°S from (a, d) the control experiment (years 1–100); (b, e) the 4 × CO_2 experiment, (years 401–500); and (c, f) the difference (4 × CO_2-control). Contour intervals are (a), (b) 3 m s^{-1}; (c) 0.5 m s^{-1}; (d, e) 6 mb day^{-1}; and (f) 2 mb day^{-1}.

the region 2°N–2°S, 142.5°E–157.5°W) decreases by about 9%. In the model ocean, the westward equatorial ocean current decreases by 21% (Fig. 5). The less intense surface winds, wind stress, and zonal surface pressure gradient are consistent with the weaker zonal SST gradients noted earlier.

The reduced zonal SST gradient is not clearly evident in the model until about *one century* of integration (Fig. 6). This is due to internal variability in the model, the gradual buildup of the CO_2 forcing, and the long response time of the coupled ocean–atmosphere system. In contrast, the large-scale (zonally uniform) component of the tropical Pacific warming is evident after only a few decades of integration (e.g., see Fig. 2 of Knutson and Manabe 1994). The decrease in zonal wind stress and the pronounced local enhancement of precipitation over the central Pacific (Figs. 4c and 2c) have a similar temporal evolution to that of the SST gradient in Fig. 6. The implication of the long "detec-

tion timescale" for the SST gradient change is that transient experiments of relatively short duration (i.e., less than order 100 years) may not be sufficient for assessing the long-term impact of increased CO_2 on the zonal SST gradient and related climate features of the tropical Pacific. However, we note that the coupled model experiment of Meehl and Washington (1989) shows a qualitatively similar decrease in the tropical Pacific zonal SST gradient after only 30 years of integration with 2 × CO_2 forcing.

There is some resemblance between the simulated CO_2-induced changes in the time-mean tropical Pacific climate and low-amplitude ENSO warm events, although differences are also readily apparent. For example, both ENSO events and the simulated CO_2-induced changes in the mean state feature a weaker zonal SST gradient, zonal surface pressure gradient, and surface easterlies (Rasmusson and Carpenter 1981), along with enhanced precipitation over the central equatorial

(a) Control Experiment (Yrs. 1–100)

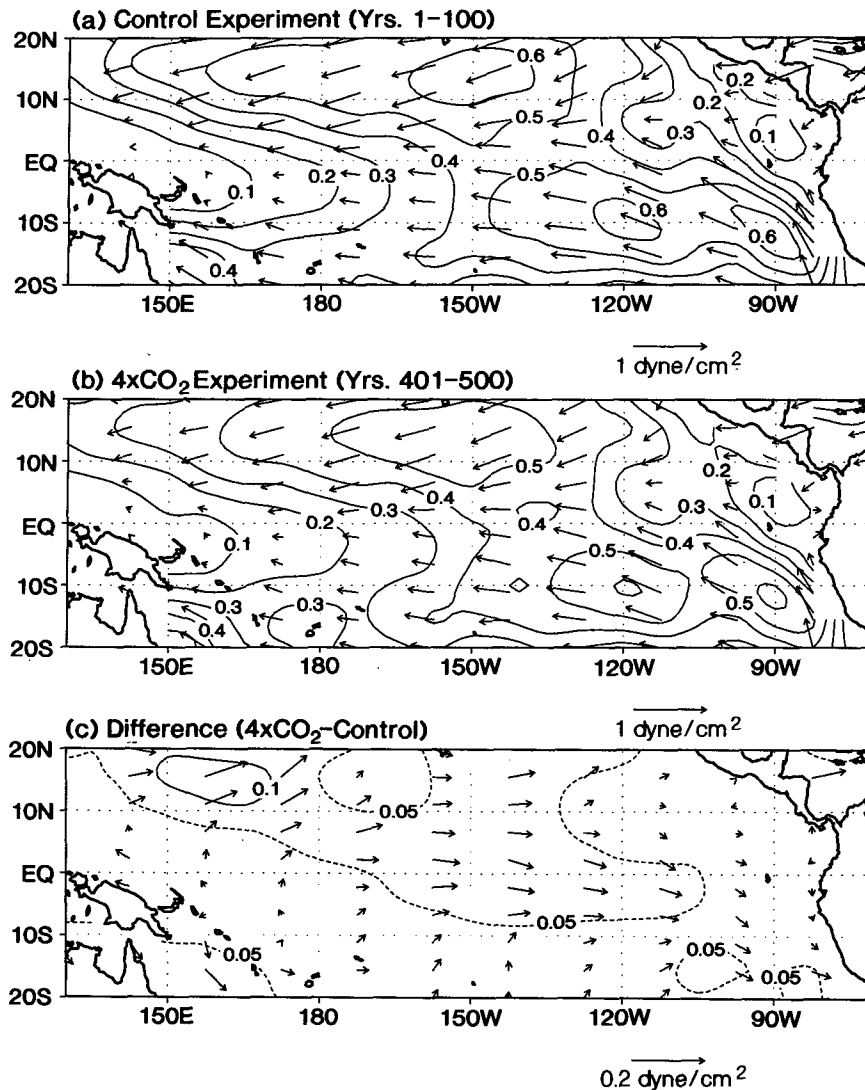## (b) 4xCO₂ Experiment (Yrs. 401–500)

(c) Difference (4xCO₂–Control)

FIG. 4. Annual mean surface wind stress components ($\overline{\tau}_x$ and $\overline{\tau}_y$) for the (a) control run (years 1–100), (b) 4 × CO₂ experiment (years 401–500), and (c) difference (b – a). Contours are for the quantity $(\overline{\tau}_x{}^2 + \overline{\tau}_y{}^2)^{1/2}$; contour intervals: (a, b) 0.1 dyn cm^{-2} and (c) 0.05 dyn cm^{-2}.

Pacific (Ropelewski and Halpert 1987). However, the warmer tropical SSTs in the central and eastern Pacific during ENSO events are typically accompanied by cooler SSTs over much of the extratropical Pacific (Pan and Oort 1983); and precipitation, while enhanced over the central Pacific, is suppressed over Indonesia and the western Pacific (Ropelewski and Halpert 1987). In contrast, the simulated CO₂-induced warming occurs throughout the Tropics and nearby extratropics, and precipitation is increased throughout the Tropics, including the western Pacific/Indonesia region.

4. Atmospheric heat budget

A surprising result from section 3 is that the time-mean rising motions over the western tropical Pacific

warm pool *decrease* slightly in intensity with increased CO₂, despite the increase of precipitation. Since one might have expected that increased precipitation and associated heating would lead to enhanced time-mean ascent, in this section the atmospheric heat balance will be examined to help interpret why the vertical motions did not intensify with the increase of precipitation.

The heat budget analysis is based on a time-averaged form of the model's temperature tendency equation (see appendix A). Figure 7a shows the annual mean heat balance in the control experiment (solid lines) for a region of pronounced precipitation over Indonesia and the western Pacific. Figure 7b shows the balance for a region of time-mean subsidence in the southeast tropical Pacific. In the western Pacific a basic three-term balance occurs: heating due to moist convection
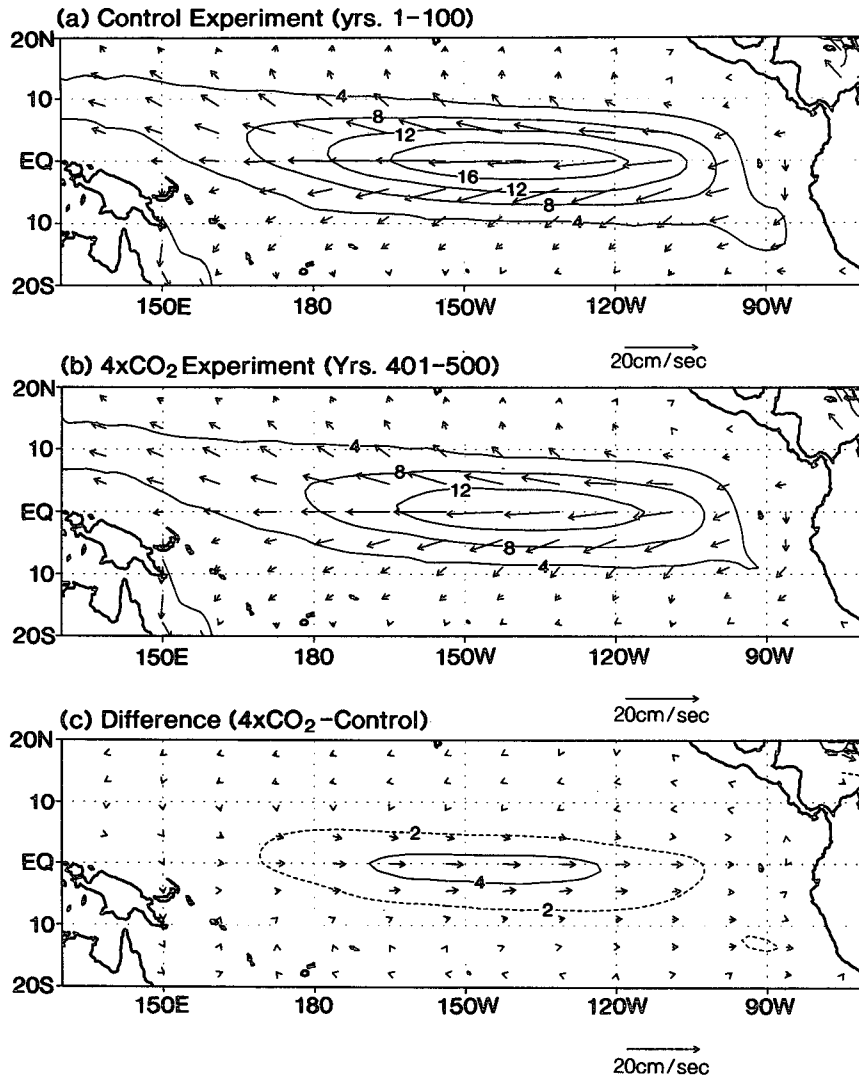
(a) Control Experiment (yrs. 1-100)

(b) 4xCO₂ Experiment (Yrs. 401-500)

(c) Difference (4xCO₂ -Control)

FIG. 5. Annual mean ocean surface-layer currents for the (a) control run (years 1–100), (b) 4 × CO₂ experiment (years 401–500), and (c) difference (b − a). Contours are for the quantity $(\bar{u}^2 + \bar{v}^2)^{1/2}$; contour intervals: (a), (b) 4 cm s⁻¹, and (c) 2 cm s⁻¹.

and condensation (roughly $+2$ K day⁻¹) is approximately balanced by dynamical and radiative cooling, both of order -1 K day⁻¹. In the eastern Pacific, the radiative cooling rate is similar to that in the west (about -1 K day⁻¹) and is balanced by dynamical *warming* (about $+1$ K day⁻¹), with moist convection and condensation playing only a minor role except near the surface. Although not shown, the contributions due to sensible heating (vertical diffusion) are large only near the surface and can be approximately inferred as a residual from the three-term balances shown.

As shown later in this section, if the model's heat balance is formulated in terms of potential temperature (θ), the dynamical cooling can be approximated by the stationary vertical advection of potential temperature ($-\bar{\omega}\partial\bar{\theta}/\partial p$). Cornejo-Garrido and Stone (1977)

analyzed the heat balance of the observed Walker circulation in terms of perturbations from the zonal mean over the tropical Pacific region. They found that as a first approximation, the longitudinal perturbation in condensation heating is balanced by the east–west perturbation in vertical velocity, which provides for relative dynamical cooling in the west and relative heating in the east. Such a balance is broadly consistent our model's heat balance over the tropical Pacific, as shown in Fig. 7.

The heat balance terms from the 4 × CO₂ experiment are depicted by dashed lines in Fig. 7. Although the basic balances are similar to the control run balance, some CO₂-induced changes are evident. In the western tropical Pacific (Fig. 7a) heating by moist convection and condensation is enhanced—primarily in the upper
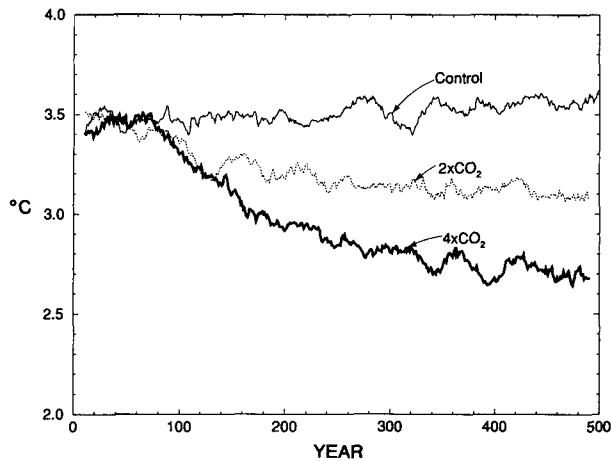
FIG. 6. Temporal evolution of the model's zonal SST gradient in the equatorial Pacific as depicted by the SST for the western Pacific (2°N–2°S, 142.5°E–157.5°W) minus that in the eastern Pacific (2°N–2°S, 142.5°–82.5°W). Shown are 20-yr running means from the control run, the 4 × CO_2 experiment, and for comparison a second transient CO_2 perturbation experiment in which CO_2 doubles over a period of 70 years and then remains fixed at 2 × CO_2 for 430 years.

troposphere—in association with the enhanced precipitation over this region (e.g., Fig. 2c). In terms of vertically integrated (140–1000 mb) heating changes (roughly depicted by the shaded regions in Fig. 7), about two-thirds of the CO_2-induced enhancement of heating by moist convection and condensation is balanced by enhanced radiative cooling; enhanced dynamical cooling offsets 18%. The remaining 16% of the "enhanced heating" (actually a decrease in the near-surface cooling by convection) is compensated by a decreased near-surface vertical diffusion of sensible heat. Over the eastern Pacific (140°–90°W), where a much smaller CO_2-induced enhancement of precipitation occurs, the enhanced radiative cooling is largely balanced by enhanced dynamical *warming*.

The longitudinal variation of the CO_2-induced changes in the primary heat budget terms is shown in Fig. 8. The heating enhancement by moist convection and condensation (Fig. 8a) has maxima over the primary tropical convection regions. The radiative cooling enhancement at 200 and 350 mb (Fig. 8b) is much more longitudinally uniform (although it has a maximum at 200 mb over the Indian Ocean and western Pacific). Because of this relatively small longitudinal variation, the radiative cooling change mainly affects the zonal mean diabatic heating, whereas the condensation heating changes contribute substantially to both the zonal mean and eddy diabatic heating response to the increased CO_2. Enhanced dynamical cooling (Fig. 8c) is important for balancing the more locally concentrated regions of enhanced condensation heating, such as that just east of the date line (180°–140°W; compare with Figs. 8a and 2c). Although not shown here, we have computed atmospheric heat balance

anomalies for the ENSO-like events from the control simulation for the central equatorial Pacific region of enhanced precipitation. In this case (and for the CO_2-induced changes in ENSO-like events), the condensation heating anomalies are primarily balanced by dynamical cooling, with radiative cooling anomalies playing a relatively minor role.

a. Radiative cooling changes

To diagnose the mechanism producing enhanced upper-tropospheric radiative cooling in the 4 × CO_2 experiment, the model was rerun for a series of "one timestep" experiments in which the temperature, mixing ratio, CO_2, and cloud distributions were selectively perturbed in various combinations to estimate the relative effect of each variable on the radiative heating
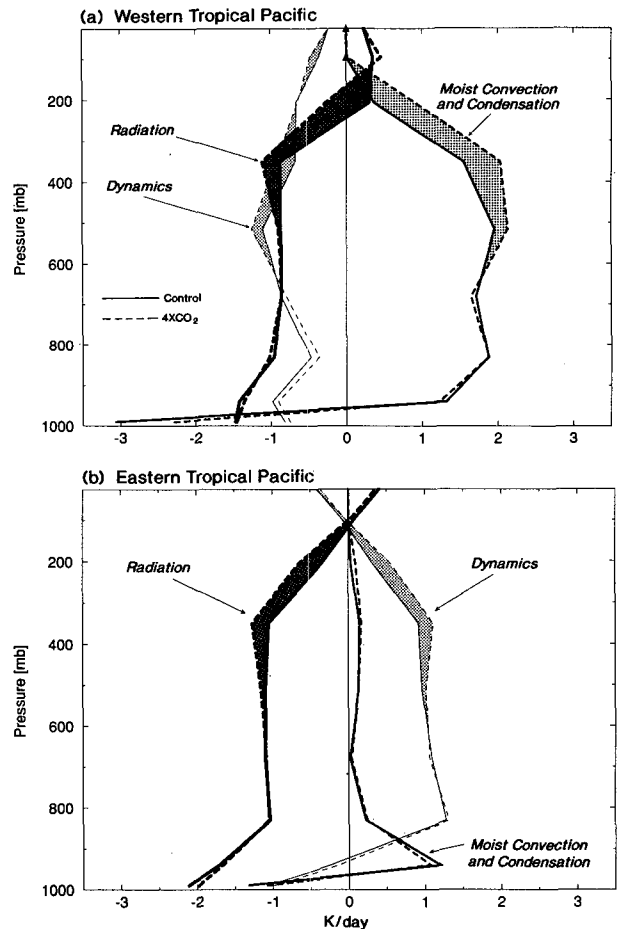
FIG. 7. Vertical profiles of temperature tendencies due to radiation (dark lines), moist convection and condensation (medium lines), and dynamical heating (light lines) for the control run, years 1–100 (solid lines) or the 4 × CO_2 experiment, years 401–500 (dashed lines). Units are kelvins per day. All values are annual means averaged over (a) the western tropical Pacific (11°N–11°S, 120°E–157.5°W); or (b) the southeast tropical Pacific (11°–20°S, 82.5°–105°W).

FIG. 8. Longitude vs pressure profiles of the changes (4 × CO_2 experiment, years 401–500 minus the control experiment, years 1–100)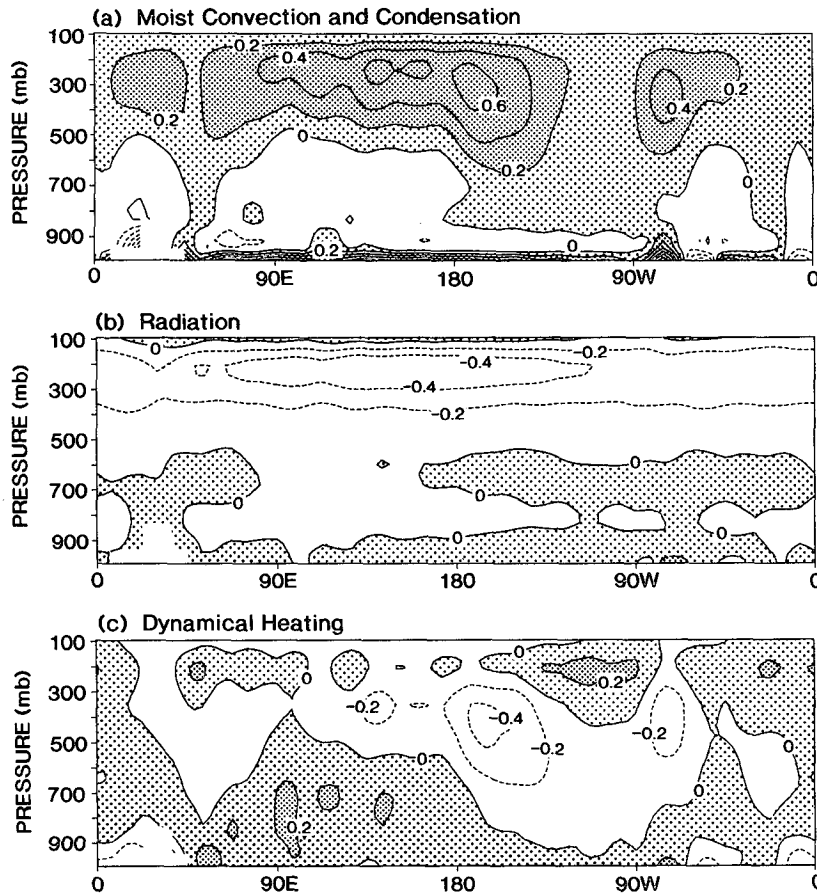 in the temperature tendencies due to (a) moist convection and condensation (b) radiation, (c) dynamical heating. Contour intervals are 0.2 K day^{-1}; positive values (relative heating) are shaded. All values are annual means, averaged 11°N–11°S.

perturbation field. The results, summarized in Table 1, show that the enhanced radiative cooling near 200 mb is due to both increased water vapor and the direct effect of upper-tropospheric warming; changes in clouds and the direct effect of CO_2 have relatively minor direct impacts on the radiative cooling rates near 200 mb. Mitchell and Ingram (1992) also found CO_2-induced increases in upper-tropospheric radiative cooling in their GCM experiment, which they attributed, also using single timestep experiments, to temperature-driven increases in upper-tropospheric water vapor.

The vertical profiles of the key driving factors for the enhanced radiative cooling (air temperature warming and large fractional increase in water vapor) are shown in Fig. 9. The ratios (4 × CO_2/Control) of the water vapor mixing ratio are shown rather than the absolute changes (4 × CO_2 − Control), because for water vapor amounts typical of the troposphere, the absorption (or emission) of longwave radiation depends almost linearly upon the logarithm of the water

vapor amount (Goody 1964). Thus, the change in absorption is more closely related to the ratio of the water vapor amounts than to the absolute difference. Since this ratio is largest (about 2.5) near 200 mb, the emission by water vapor increases substantially at that level. With regard to the temperature changes, the warming at 350 and 205 mb (about +8°C) is greater than that at lower levels; hence, the temperature-driven radiative cooling from these layers is substantially enhanced.

The increase of the air temperature warming with height through the troposphere is an effect of moist convection, which keeps the vertical lapse of temperature in the model Tropics close to the moist adiabatic rate, making the model's lapse rate (i.e., $-dT/dz$) less in a warmer atmosphere. This leads to a larger fractional increase in water vapor in the upper troposphere than near the surface. In addition, the fractional increase in water vapor mixing ratio (per degree of warming) is larger for cooler temperatures (as occur in the upper troposphere) than for warmer lower-tro-

TABLE 1. CO_2-induced changes in the temperature tendency due to radiation, $\delta T_{rad}/\delta t$, at the model sigma level 0.205 × surface pressure (see appendix A). Each case below is based on an ensemble of 100 one-time step runs using 1 January initial data from the CO_2-perturbation (years 401–500) and control experiments. Effects are estimated by Δ, which is computed as the ensemble of the runs with a single variable (e.g., temperature) changed from control run to 4 × CO_2 run conditions minus the ensemble with unperturbed control run conditions. The "net effect" is based on changing all four variables simultaneously; the fact that it differs from the sum of the individual effects indicates the presence of interaction between the different variables. Results are zonal means, averaged 20°N–20°S, in kelvins per day.

Variable altered	$\Delta \dfrac{\delta T_{rad}}{\delta t}$ (K day^{-1})
Temperature	−0.237
Mixing ratio of H_2O	−0.290
CO_2	−0.021
Clouds	−0.019
Sum of individual effects	−0.568
Net effect of all variables	−0.409

pospheric temperatures. These effects were also noted by Mitchell and Ingram (1992). The small changes in relative humidity have a relatively minor effect on the vertical profile of fractional changes in water vapor. The large fractional increases in upper-tropospheric water vapor in our model are consistent with the GCM results of Mitchell and Ingram (1992) and DelGenio et al. (1991) and with the preliminary results of a warming experiment using a limited-area, cumulus ensemble model with fixed large-scale vertical velocity (Lau et al. 1993).

b. Dynamical cooling changes

The nature of the CO_2-induced changes in the dynamical cooling is explored in Fig. 10. In order to simplify the analysis, changes in the stationary vertical advection of potential temperature ($-\bar{\omega}\partial\bar{\theta}/\partial p$) are examined (see appendix A). As shown in Fig. 10 the total dynamical cooling in terms of potential temperature (diamonds) is roughly equivalent to $-\bar{\omega}\partial\bar{\theta}/\partial p$ alone (thin solid line) for the western tropical Pacific region. Differences between the total dynamical cooling and $-\bar{\omega}\partial\bar{\theta}/\partial p$ in Fig. 10 are due to the effects of horizontal advection (stationary and transient) and transient vertical advection of potential temperature.

The thin and thick solid curves in Fig. 10 show $-\bar{\omega}\partial\bar{\theta}/\partial p$ from the control and 4 × CO_2 experiments, respectively, while the remaining two (dashed) curves in the figure illustrate the effect on $-\bar{\omega}\partial\bar{\theta}/\partial p$ of changing either the $\partial\bar{\theta}/\partial p$ or $\bar{\omega}$ distribution alone, keeping the other variable fixed. The results show that CO_2-induced changes in $-\partial\bar{\theta}/\partial p$ (the static stability) act to enhance the dynamical cooling. The primary effect of changes in $\bar{\omega}$ is to shift the cooling profile upward slightly, but with little impact on the vertically integrated cooling.
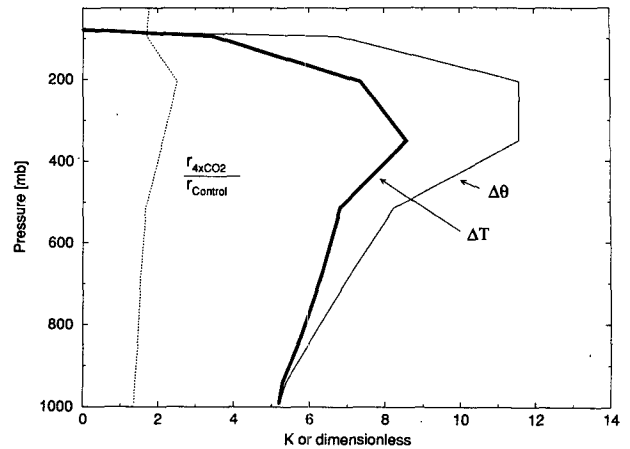

FIG. 9. Vertical profiles of the ratio (4 × CO_2 divided by Control) for the water vapor mixing ratio; absolute changes in temperature (4 × CO_2 − control) in kelvin; and absolute changes in potential temperature (4 × CO_2 − Control) in kelvin. Values are annual-mean zonal means (11°N–11°S), based on years 1–100 of the control experiment and years 401–500 of the 4 × CO_2 experiment.

As is shown in Fig. 9, the CO_2-induced increase in potential temperature is largest in the upper troposphere, indicating an increase of the time-mean static stability through most of the tropical troposphere. As discussed above, this increased static stability can be qualitatively understood in terms of the behavior of moist adiabatic lapse rates, toward which the model temperature profile is adjusted via moist convective
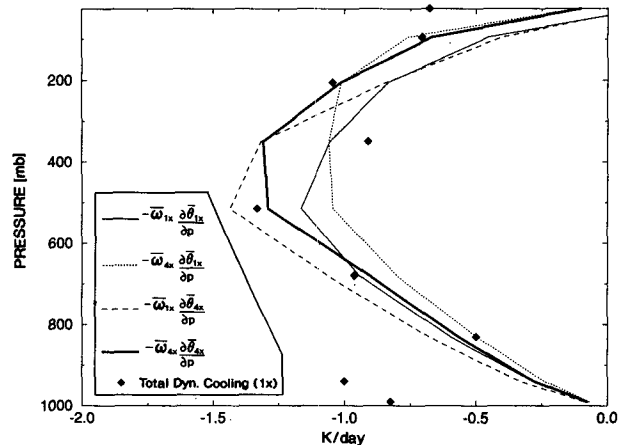
FIG. 10. Vertical profiles of: the total dynamical heating rate from the control experiment, including horizontal, vertical, stationary, and transient contributions (diamonds); and the term $-\bar{\omega}\partial\bar{\theta}/\partial p$ from the control experiment (thin solid line) or 4 × CO_2 experiment (thick solid line). Dotted line: $-\bar{\omega}\partial\bar{\theta}/\partial p$, computed using $\bar{\omega}$ from the 4 × CO_2 experiment and $\partial\bar{\theta}/\partial p$ from the control experiment. Dashed line: $-\bar{\omega}\partial\bar{\theta}/\partial p$, computed using $\bar{\omega}$ from the control experiment and $\partial\bar{\theta}/\partial p$ from the 4 × CO_2 experiment. Values are annual means for the area 11°N–11°S, 120°E–157.5°W, based on data from years 1–100 of the control experiment and years 401–500 of the 4 × CO_2 experiment.

TABLE 2. Surface energy balance at the atmosphere–ocean interface in the western equatorial Pacific (7°N–7°S, 150°–172.5°E). Results are expressed as net surface energy flux gains (in W m^{-2}) for the control (years 1–100) and 4 × CO_2 (years 401–500) experiments. Key: SW: shortwave radiation; LW: longwave radiation; SH: sensible heat flux; LH: latent heat flux; and Q: net surface energy flux gain. The surface energy balance can be expressed as SW + LW + SH + LH = Q.

Term	Control	4 × CO_2	4 × CO_2 − Control	Percent change in magnitude
SW	185	190	+5	+3%
LW	−53	−43	+10	−18%
SH	−18	−14	+4	−23%
LH	−123	−142	−19	+15%
Q	−10	−10	+0.2	−2%

adjustment. Owing to this increased static stability, the dynamical cooling by vertical velocities of a given magnitude tends to be enhanced in a warmer atmosphere, especially in the moist Tropics.

Although not shown here, in the southeast tropical Pacific region analyzed in Fig. 7b, much of the enhanced dynamical warming is also attributable to increased time-mean static stability (via $-\bar{\omega}\partial\bar{\theta}/\partial p$). In fact, the time-mean subsidence ($\bar{\omega}$) is generally weaker in the 4 × CO_2 experiment in this region and thus does not contribute to enhancing the dynamical warming.

An intensification of the upper-tropospheric time-mean vertical velocities can also be inferred from Fig. 10. This is associated with the slightly higher penetration of tropical cumulus convection (and upward shift in high cloudiness) in the CO_2-warmed tropical troposphere, as found by Wetherald and Manabe (1988) and Mitchell and Ingram (1992). These vertical motion changes are consistent with a slight deepening of the model's Walker Circulation, which can also be inferred in Fig. 3f.

Thus, over the warm pool, enhanced radiative and dynamical cooling (the latter associated with time-mean static stability changes) compensate the enhanced heating by moist convection and condensation in the 4 × CO_2 experiment, despite the fact that the time-mean vertical motions in the rising branch of the Walker circulation fail to intensify. Similarly, in the cooler eastern Pacific, the enhanced radiative cooling is compensated by enhanced dynamical warming, which occurs despite generally weaker time-mean subsidence.

5. Surface energy balance

In this section, the surface energy balance is analyzed to further diagnose the CO_2-induced increases in evaporation and precipitation and the reduction of the zonal SST gradient in the equatorial Pacific.

a. Western tropical Pacific

The model's surface energy balance at the atmosphere–ocean interface is shown in Table 2 for the western Pacific warm pool region. Qualitatively similar results are obtained for the eastern tropical Pacific (not shown). For the 4 × CO_2 experiment, the latent heat flux to the atmosphere is 19 W m^{-2} greater (+15%) than in the control, whereas the sensible heat flux decreases by 4 W m^{-2} (−23%). The decreased sensible heat flux is associated with the reduced surface to air temperature difference in the 4 × CO_2 run (SST increases 4.2 K, while surface air temperature increases 4.7 K). The latent heat flux increases despite the smaller surface to air temperature difference due in large part to the nonlinear dependence of saturation mixing ratios on temperature. Owing to this effect the saturation mixing ratio at the surface increases more than the mixing ratio of surface-layer air, leading to enhanced evaporation. The enhanced surface heat loss by evaporation is balanced mainly by a net radiative energy flux gain of 15 W m^{-2}, which includes both decreased net upward longwave radiation (10 W m^{-2}) and enhanced net downward shortwave radiation associated with cloud changes (5 W m^{-2}). There is little change in the net ocean–atmosphere heat flux in this region in response to the increased CO_2.

The surface energy balance also provides a useful perspective for interpreting the increase of tropical precipitation with increased CO_2. Precipitation and evaporation increase by roughly the same fractional amount in the Tropics, indicating that the increase of tropical precipitation is largely driven by the increase of evaporation within the Tropics. Thus, the increased tropical precipitation in the warmer climate may be interpreted as a consequence of the model ventilating more heat to the atmosphere via enhanced evaporation. As described above, the increased evaporation is balanced primarily by the enhanced net downward radiative flux at the surface.

As background for the subsection that follows, the heat balance for the ocean model's surface layer (as

TABLE 3. Ocean model surface-layer energy balance in the western equatorial Pacific (7°N–7°S, 150°–172.5°E). Results are net surface layer energy flux gains (in W m^{-2}) for the control (years 1–100) and 4 × CO_2 (years 401–500) experiments. Key: Q: surface energy flux gain (see Table 2); FA: surface energy flux adjustment; and A: energy flux gain due to ocean advection and diffusion. The flux adjustment represents the energy flux that must be added to that computed in the atmospheric component of the coupled model in order to obtain a satisfactory simulation of the observed SST climatology.

Term	Control	4 × CO_2	4 × CO_2 − Control	Percent change in magnitude
Q	−10	−10	+0.2	−2%
FA	23	23	—	—
A	−13	−13	−0.2	+1%

opposed to the atmosphere–ocean interface discussed above) is presented in Table 3 for the western Pacific warm pool region (see also Lau et al. 1992). The balance can be expressed as $Q + FA + A \approx 0$, where Q is the net heat flux gain for the layer at the ocean–atmosphere interface (discussed above), FA is the heat flux adjustment (see section 2), and A is the heat flux gain for the region via advection and diffusion. The surface layer energy flux loss to the atmosphere is about 10 W m^{-2} in both the 4 × CO_2 and control experiments. The ocean surface layer gains 23 W m^{-2} through the model heat flux adjustment (which is specified to be identical in both experiments). Thus, the ocean surface layer in the warm pool region has a net energy flux gain of 13 W m^{-2}, which is balanced by ocean heat transport loss of about 13 W m^{-2} in both the 4 × CO_2 and control experiments.

b. Differential (west minus east) surface energy balance

In this section, we investigate the decrease in the time-mean zonal SST gradient (i.e., in the west–east difference in SST along the equator) by analyzing the west–east contrast in each of the ocean surface layer energy balance components, along with the changes in these components with a quadrupling of CO_2. The results are summarized in Fig. 11. In the control run, ocean advection and diffusion (A), along with the heat flux adjustment (FA), cool the eastern Pacific surface layer relative to the western Pacific and thus act to sustain the existing SST gradient. On the other hand, evaporation, net radiation (particularly shortwave), and sensible heat flux all act to cool the western Pacific relative to the eastern Pacific and thus act to inhibit further growth in the SST gradient. At "equilibrium" conditions in the model, a state is reached in which the terms that create the SST gradient (i.e., advection/ diffusion and heat flux adjustment) are balanced by the terms that damp the gradient (i.e., net radiative, sensible, and latent heat fluxes).

With a quadrupling of CO_2 a new "equilibrium" is reached in which the west–east contrast in SST is reduced by 21%. Similarly, the ocean temperature advection/diffusion contrast, which acts to sustain the SST gradient, is reduced by 23% and the net radiative and sensible heat flux damping terms are reduced by 21% and 29%, respectively (Fig. 11). Thus, the fractional change of each of these terms is roughly the same as the fractional change of the SST gradient. On the other hand, the west–east contrast in evaporation decreases by only about 4%, despite the 21% decrease in the SST gradient. In other words, the evaporative damping per degree of west–east SST contrast is enhanced in the 4 × CO_2 experiment.

The behavior of the east–west contrast in evaporation can be qualitatively understood through an analysis of the model's ocean surface evaporation equation:
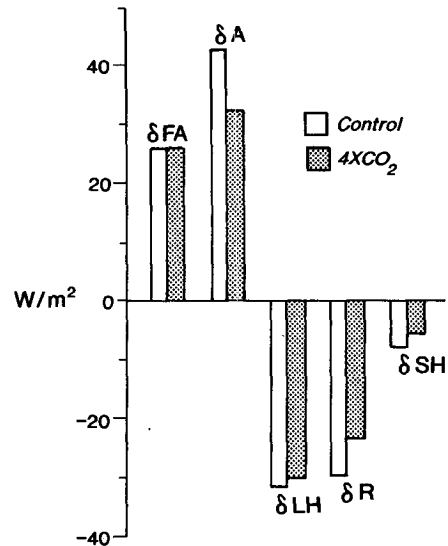

FIG. 11. Differential (δ, or west minus east) energy flux gains for the model ocean surface layer from the (solid) control experiment (years 1–100) and the (shaded) 4 × CO_2 experiment (years 401–500) in watts per square meter. $\delta f = f(2°N–2°S, 142.5°E–157.5°W)$ minus $f(2°N–2°S, 142.5°–82.5°W)$. Key: FA: heat flux adjustment (see Table 3 caption); A: temperature advection and diffusion; LH: latent heat flux (evaporation); R: net radiative flux; and SH: sensible heat flux.

$$\text{evap} = \rho C_d W_1 \{ r_{sat}(T_{sfc}) - h_1 r_{sat}(T_1) \}. \quad (1)$$

In (1), ρ is the density of air, C_d is the constant drag coefficient, W is the wind speed, r is the mixing ratio, T is the temperature, h is the relative humidity (r/r_{sat}), and the subscripts $_{sat}$, $_{sfc}$, and $_1$ represent saturation, surface, and the lowest atmospheric model level (at pressure = 0.99 × surface pressure), respectively.

First, we consider why evaporation is larger in the western equatorial Pacific than in the eastern equatorial Pacific in the control simulation. The $\overline{h}_1$ difference between the west and east is only a few percent and the mean winds are stronger in the east than in the west; therefore, for simplicity we focus on east–west differences in the quantity $r_{sat}(\overline{T_{sfc}}) - \overline{h}_1 r_{sat}(\overline{T_1})$, obtained using time-mean temperatures from the control run and assuming a constant value of 0.9 for $\overline{h}_1$. Under these assumptions, $r_{sat}(\overline{T_{sfc}}) - 0.9 r_{sat}(\overline{T_1})$ is almost 60% higher in the west than in the east. (In comparison, evaporation is about 40% higher in the west.) The west–east contrast in $r_{sat}(\overline{T_{sfc}}) - 0.9 r_{sat}(\overline{T_1})$ is attributable to both the warmer basic-state temperatures in the west and the larger air–sea temperature difference ($\overline{T_{sfc}} - \overline{T_1}$) in the west, with both effects being of comparable importance. Thus, we conclude that both of these effects are also important for producing the west–east contrast in evaporation in the control simulation.

As shown in Fig. 11, the west–east contrast in evaporation is approximately the same in the 4 × CO_2 "equilibrium" state as in the control run, despite the

weaker west–east contrast in temperature. To illustrate how this occurs, we note that for a uniform 1 K increase in $\overline{T}_{sfc}$ and $\overline{T}_1$ in both the west and east, the west–east difference in $r_{sat}(\overline{T}_{sfc}) - 0.9r_{sat}(\overline{T}_1)$ increases by 5.6%, due to the temperature dependence of dr_{sat}/dT via the Clausius–Clapeyron equation. This illustrates how the evaporative damping of the zonal SST gradient (i.e., the west–east difference in evaporative cooling) increases with increasing temperature due to the Clausius–Clapeyron dependence alone. However, using the actual $\overline{T}_{sfc}$ and $\overline{T}_1$ values from the $4 \times CO_2$ and control experiments, $r_{sat}(\overline{T}_{sfc}) - 0.9r_{sat}(\overline{T}_1)$ is approximately unchanged, despite this Clausius–Clapeyron effect, because the west–east difference in temperature is reduced. Thus, the model adjusts to the warmer climate by decreasing the zonal SST gradient, which provides for an "offsetting reduction" of the what otherwise would have been an enhanced west–east evaporation differential. In this manner, enhanced evaporative damping of the zonal SST gradient, due to the warmer climate, plays an important role in reducing the SST gradient.

The heat flux adjustment, which acts to *sustain* the model's zonal SST gradient, is identical for both the control and $4 \times CO_2$ experiments. Thus, its contribution to the balance *per degree of SST contrast* is also enhanced in the $4 \times CO_2$ experiment because the west minus east SST contrast is smaller. Suppose, however, that the flux adjustment (or the processes that it represents) behaved in a similar manner to the net radiation, ocean heat transport, and sensible heat flux terms (i.e., that it decreased by roughly the same fractional amount as the SST gradient). In that case, one might expect the SST gradient to be even more sensitive to increased CO_2 than was found with the present model. This suggests, in other words, that an even larger CO_2-induced reduction in the zonal SST gradient may occur in a similar model in which no heat flux adjustment is used.

6. Atmospheric moisture budget

To examine how additional moisture is supplied to the upper troposphere for the increased condensation heating despite a decreased intensity of the time-mean vertical motions, the model's atmospheric moisture budget is analyzed in this section using the time-averaged form of the mixing ratio tendency equation (see appendix A).

Key features of the model's climatological atmospheric moisture budget over the western tropical Pacific region are shown in Fig. 12. Referring first to the solid curves (control experiment), the time-mean mixing ratio tendency due to moist convection and condensation is negative at all levels, as moisture is removed from the atmosphere as precipitation. According to Fig. 12, in the middle- and upper-troposphere transient advection (primarily transient vertical

advection—not shown) supplies most of the water vapor to balance the moisture removal by moist convective adjustment and saturation, although stationary advection also contributes to the balance. In the lower troposphere, vertical diffusion of waver vapor evaporated from the surface is the largest source of water vapor; it is balanced primarily by a transient advection sink. Stationary advection (moisture source) and moist convection and condensation (moisture sink) also make significant, though smaller, contributions to the lower-tropospheric moisture balance.

The corresponding moisture budget terms from the $4 \times CO_2$ experiment are represented by the dashed lines in Fig. 12. A comparison with the control run curves shows that most of the enhanced moisture removal by moist convection and condensation occurs in the upper troposphere. If adjusted to have heating units ($K \ day^{-1}$), the profile of CO_2-induced moisture removal enhancement corresponding to Fig. 12 is similar to the CO_2-induced enhancement of heating by moist convection and condensation shown in Fig. 8. The enhanced moisture removal in the upper troposphere is balanced by both enhanced transient and stationary advection, with the transient advection having the greater relative effect. In the lower troposphere, the enhanced vertical diffusion source is balanced primarily by an enhanced transient advection sink.

Although the CO_2-induced changes to the stationary advection term are small, they illustrate how the vertical moisture advection can be enhanced even with weaker vertical motions. Enhanced time-mean moisture gradients lead to enhanced moisture advection, whereas changes in the time-mean circulation (i.e., slightly weaker vertical motions) act to reduce this enhance-
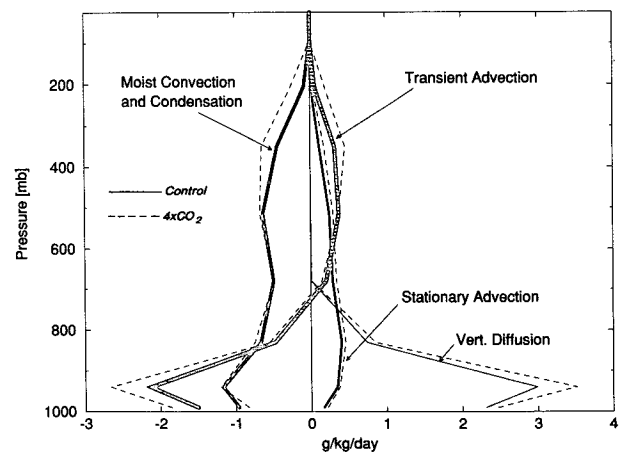
FIG. 12. Vertical profiles of mixing ratio tendencies due to vertical diffusion (thinnest lines); stationary advection (medium thin) moist convection and condensation (medium thick); and transient advection (thickest lines). Solid lines show terms for the control experiment, (years 1–100), and dashed lines are for the $4 \times CO_2$ experiment (years 401–500) (Units: $g \ kg^{-1} \ day^{-1}$). All values are annual means, averaged over 11°N–11°S, 120°E–157.5°W.

ment. The enhanced time-mean vertical moisture gradients result from the much larger *absolute* CO_2-induced increases in water vapor content in the lower troposphere compared to the upper troposphere. This difference occurs despite the larger *fractional* increase in water vapor in the upper troposphere noted previously. The stationary advection term has been analyzed in detail, but the transient advection term has not. This is because high-frequency transient vertical motion and moisture data from the experiments are not available, so the relative effects of water vapor gradient fluctuations and circulation fluctuations on the changes in transient moisture advection cannot be determined at present.

In broad terms, the model's stationary moisture advection response, where a relatively unchanged (or slightly weakened) circulation acts upon increased moisture gradients to produce enhanced moisture advection and precipitation, is qualitatively similar to the global-scale response of the Goddard Institute for Space Studies (GISS) GCM to a uniform sea surface warming (Del Genio et al. 1991).

In section 3, we found that total precipitable water vapor increases by a much larger fractional amount than precipitation with increased CO_2. From the viewpoint of the surface energy balance (section 5a), the fractional increase of precipitation is similar to the fractional increase of evaporation, and the evaporation increase provides the primary balance for the increase of net downward radiative flux at the surface. Nevertheless, from the viewpoint of moisture convergence, one might have expected that the fractional increases in precipitation (or $P - E$) would have been more similar to the fractional increase in water vapor content. Here we attempt to elaborate on why this does not occur in the model based on a highly simplified analysis of the available data from the experiments. Since transient data are not explicitly available from the experiments, here only the stationary moisture convergence term $\langle -\bar{r}\bar{\delta} \rangle$ is examined, where r is mixing ratio, δ is divergence, the overbar represents the time mean, and $\langle \ \rangle$ is the area-averaged vertical integral. We will illustrate why the stationary moisture convergence also increases by a much smaller fractional amount than does total precipitable water ($\langle \bar{r} \rangle$) for the western tropical Pacific. A more complete analysis of the problem will require examination of transient terms using data archived in a future set of experiments.

In the model, $\langle -\bar{r}\bar{\delta} \rangle$ increases by 16% in the 4 $\times CO_2$ experiment over the region 11°N–11°S, 120°E–157.5°W. This is comparable to the increase in precipitation (14%), evaporation (15%), and $P - E$ (12%), but much smaller than the increase in $\langle \bar{r} \rangle$ (44%). If the convergence field from the control run is combined with the moisture field from the 4 $\times CO_2$ run, the resulting term $\langle -\bar{r}_{4\times CO_2}\bar{\delta}_{1\times CO_2} \rangle$ is 35% larger than the control run term ($\langle -\bar{r}_{1\times CO_2}\bar{\delta}_{1\times CO_2} \rangle$), indicat-

ing the large effect of the increased moisture alone. However, since including moisture *and circulation* changes (i.e., $\langle -\bar{r}_{4\times CO_2}\bar{\delta}_{4\times CO_2} \rangle$) results in a much smaller increase (+16% versus +35%), it is clear that weakened circulation plays an important role in limiting the increase of $\langle -\bar{r}\bar{\delta} \rangle$ to only 16%. The remainder of the difference (35% versus 44%) is due to the nonuniform distribution of the fractional increase in water vapor (e.g., the fractional increase in mixing ratio increases with height through the troposphere). The net effect of the nonuniform fractional changes can be seen by noting that if the mixing ratio were increased everywhere in the domain by 44%, the modified term $\langle -\bar{r}_{4\times CO_2}\bar{\delta}_{1\times CO_2} \rangle$ would have been 44% larger than the control run term, rather than only 35% larger. The results of our simplified analysis are consistent with Mitchell et al. (1987), who inferred that the difference in the fractional changes of $P - E$ and water vapor in their model was due to circulation changes and a nonuniform distribution of the fractional changes in specific humidity.

7. Discussion and conclusions

The results in this study indicate that the time-mean zonal overturning atmospheric circulation in the tropical Pacific region fails to intensify with increased CO_2. Despite a 15% enhancement of precipitation over the western tropical Pacific, the time-mean upward motion in the rising branch region of the Walker Circulation *decreases* slightly in intensity. In the central equatorial Pacific, the zonal SST gradient decreases by about 20%, the surface easterly wind stress decreases by 15%, and precipitation increases by about 25%. The CO_2-induced changes in the model's large-scale tropical precipitation climatology are comparatively small, considering the dramatic increase in the area of the world's ocean surface with SST exceeding 28°C. This results suggests that 28°C is not a *universally applicable* "threshhold temperature" for large-scale tropical convection but rather that pronounced tropical convective activity will tend to occur in locations where SSTs are *warmer than in surrounding regions.*

a. Lack of circulation intensification

A surprising result from the analysis is the lack of intensification of the zonal overturning circulation, despite increased condensation heating over the warm pool. Although the analysis of the heat, moisture, and surface energy budgets cannot determine causality as to why the circulation does not intensify in response to increased CO_2, it does demonstrate how the model satisfies heat, moisture, and energy balance constraints without such an intensification. Specifically, three factors were found that are important for interpreting this aspect of the model's response.

1) Much of the additional vertically integrated heating due to enhanced moist convection and con-

densation over the warm pool is offset by enhanced radiative cooling in the upper troposphere near 200 mb. The radiative cooling enhancement is due to both the large warming and to the large fractional increase in water vapor (150% increase) in the upper troposphere. As a result, the increase in emission from the upper troposphere exceeds the absorption of radiation from surrounding atmospheric layers, where the increases in both temperature and emissivity are smaller.

2) Increased time-mean static stability $(-\partial\bar\theta/\partial p)$ leads to enhanced dynamical cooling (via $-\bar\omega\partial\bar\theta/\partial p$), which compensates for most of the remaining time-mean heating enhancement from moist convection and condensation. The increased time-mean static stability is an effect of moist convection, which keeps the lapse rate in the model close to the moist adiabatic rate, making $-\partial\bar\theta/\partial p$ larger in a warmer climate.

3) Enhanced evaporative damping of the zonal SST gradient in the warmer basic state (due to the nonlinear temperature dependence of saturation mixing ratios) leads to a reduced SST gradient. The diminished SST gradient is consistent with weaker surface easterly wind stress in the central and eastern Pacific and in turn with the slightly less intense zonal overturning circulation.

A relatively coarse resolution is used for the coupled model simulations due to the large computational requirements of the long-term coupled integrations. To make a preliminary assessment of the impact of low resolution on the atmospheric heat balance results, the heat balances have been reexamined using an atmospheric model with twice the horizontal resolution coupled to a mixed-layer ocean (appendix B). The results for the western Pacific region show that both the radiative cooling and static stability effects also occur in the higher horizontal resolution model. One distinction between the results of the two sets of experiments is that in the high-resolution case the net dynamical cooling enhancement is larger than the radiative cooling enhancement. This is apparently due to the stronger overall condensation heating/dynamical cooling rates (compared with the radiative cooling rates) in the higher-resolution model and also to the CO_2-induced intensification of rising motions in the upper troposphere due to the deeper penetration of tropical convection (which is present in both the high- and low-resolution models). Nevertheless, even in the high-resolution model, the vertical motion changes contribute only about one-half as much as the static stability changes to enhancing the primary dynamical cooling term $(-\bar\omega\partial\bar\theta/\partial p)$ and offset only about 25% of the condensation heating enhancement. Thus, for both high- and low-resolution models, most of the enhanced condensation heating is not compensated by changes in vertical motions, but rather by enhanced radiative and dynamical cooling, with the latter being induced primarily by increased static stability.

With regard to time-mean *subsidence* regions the radiative cooling and static stability effects are also important for the heat balance changes (for both model resolutions). Over the relatively cool southeast tropical Pacific, changes in condensation heating are much smaller than in the western Pacific. In this region, the enhanced radiative cooling is balanced primarily by enhanced dynamical *warming,* again due in large part to the increased time-mean static stability.

b. The time-mean response versus the ENSO response

There are several similarities and relationships between the impact of increased CO_2 on the model's time mean circulation and its impact on ENSO-like phenomena in the model (Knutson and Manabe 1994). For both the time-mean climate and the model ENSO, enhanced precipitation (or precipitation anomaly) occurs, but the additional condensation heating is not balanced primarily by a more intense zonal overturning circulation (or circulation anomaly). Rather, the dynamical cooling (or cooling anomaly) is enhanced largely due to increased time-mean static stability. For both ENSO and the time-mean climate, enhanced evaporative damping in the warmer climate plays an important role in *reducing* the magnitude of SST variations (either the east–west contrast for the time-mean SST or the amplitude of the interannual ENSO-like fluctuations).

In terms of relationships between the response of the time-mean climate and the response of the model ENSO to increased CO_2, the 20% decrease in the time-mean zonal SST gradient discussed in the present study is one of the important factors contributing to the reduced amplitude of the ENSO-like SST fluctuations (along with enhanced evaporative damping of the SST anomalies). This is because with a smaller time-mean zonal SST gradient, zonal ocean surface current anomalies of a given magnitude produce a smaller temperature tendency during the model's ENSO-like events (see also Lau et al. 1992).

We have noted in this study that the reduction in the time-mean zonal SST gradient is not clearly evident until about one century of model integration. The implication of this result is that coupled model CO_2 experiments of relatively short duration (i.e., less than order 100 years) may not be sufficient for assessing the long-term impact of altered CO_2 on the zonal SST gradient and related climate features of the tropical Pacific region.

c. Paleotemperature perspective

Some may question whether the tropical SST warming of $4°-5°C$ computed in our model with $4 \times CO_2$ is plausible in light of existing paleoclimatic evidence. CLIMAP's (1981) reconstruction of low-latitude SSTs

tropical rainfall is somewhat larger with R30 (see their Fig. A2).

Given that the tropical precipitation (condensation heating) is stronger and more confined to distinct regions in the R30 simulation, it is of interest to consider what impact the use of an R30 model has on the main conclusions of our paper. Here, the heat balance changes in the R30 simulations are briefly investigated and compared with the changes from the R15 simulation. A slight CO_2-induced reduction of the zonal Pacific SST gradient occurs the R30 mixed-layer model, although it is not examined in detail since the mixed layer ocean model's response is greatly constrained by the fixed oceanic heat transport assumption.

Figure B1 shows the annual mean atmospheric heat budgets for the western tropical Pacific region from the R30 experiments. Note that despite the smaller (2 × CO_2) warming in the R30 experiment, the enhancement of heating by moist convection and condensation is comparable to that in the 4 × CO_2 R15 experiments (Fig. 7a). The enhancement of upper-tropospheric radiative cooling found in the R15 experiment is clearly present in the high-resolution experiments; the absolute change is smaller due to the smaller (2 × CO_2) warming. The enhancement of vertically integrated (131–1000 mb) dynamical cooling is relatively more pronounced in the R30 experiments: it accounts for about 55% of the cooling enhancement, whereas enhanced radiative cooling accounts for about 40%. (For the low-resolution model, dynamical and radiative cooling accounts for 18% and 67% of the cooling enhancement, respectively.)

Changes in the term $-\bar{\omega}\partial\bar{\theta}/\partial p$ have also been investigated (not shown), as was done for the low-resolution model in Fig. 10. As in the R15 experiments, changes in the potential temperature gradient contribute more to the enhancement of $-\bar{\omega}\partial\bar{\theta}/\partial p$ than do changes in vertical velocities. However, one difference between the two sets of experiments is that in the R30 experiments the time-mean vertical velocities account for about one-third of the enhancement of $-\bar{\omega}\partial\bar{\theta}/\partial p$ (and are sufficient to offset 25% of the condensation heating enhancement). On the other hand, in the low-resolution model, changes in $\bar{\omega}$ have almost no net impact on the vertically integrated cooling in the western tropical Pacific.

Vertical motion profiles for the western Pacific region (not shown) indicate that in the high-resolution model, time-mean rising motion is slightly intensified in the upper troposphere (due to deeper penetration of convection) but is nearly unchanged in the lower troposphere. In contrast, in the low-resolution model, time-mean vertical motions are also stronger in the upper troposphere, but they are *weaker* in the lower troposphere. In the time-mean descent region over the eastern tropical Pacific (11°–20°S, 82.5°–105°W), the time-mean subsidence is slightly weaker (stronger) in the lower (upper) troposphere for both resolutions. For
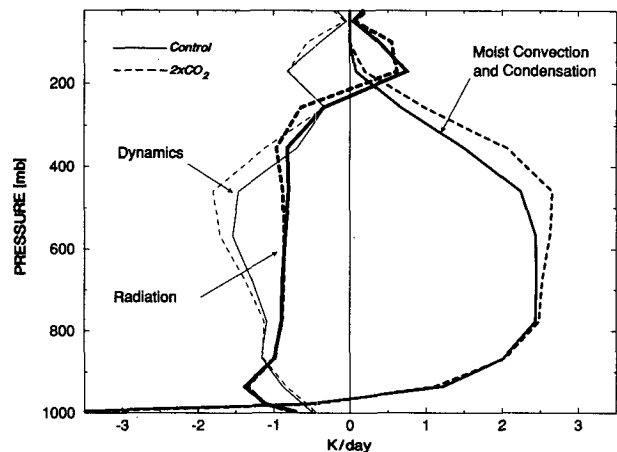

FIG. B1. Vertical profiles of temperature tendencies due to radiation (dark lines), moist convection and condensation (medium lines), and dynamical heating (light lines) for the control (solid) or 2 × CO_2 (dashed) experiments with the R30 mixed-layer model (see appendix B text). Units are kelvin per day. All values are decadal means (all seasons), averaged over 10°N–10°S, 120°E–157.5°W.

both resolutions, the surface winds over the central and eastern Pacific weaken slightly with increased CO_2 (although differences in the ocean model formulations make comparisons of the surface wind and SST changes more problematic).

In summary, in both sets of experiments most of the CO_2-induced enhancement of heating by moist convection and condensation is primarily balanced by the radiative cooling and enhanced static stability, rather than by intensified time-mean vertical velocities. In both sets of experiments, the zonal overturning circulation fails to intensify substantially despite the substantial increase of condensation heating over the warm-pool region (although vertical motions do intensify slightly in the upper troposphere in both experiments due to deeper penetration of tropical convection). Therefore, we conclude that the main findings of the low-resolution analysis (except for the slight *weakening* of the lower-tropospheric vertical motions over the warm pool) are generally supported by the simulations with the R30 model.

REFERENCES

Broccoli, A. J., and S. Manabe, 1990: Can existing climate models be used to study anthropogenic changes in tropical cyclone climate?. *Geophys. Res. Lett.,* **17,** 1917–1920.

CLIMAP Members, 1981: Seasonal reconstruction of the earth's surface at the last glacial maximum. *Geol. Soc. Amer. Map Chart Ser.,* **36,** 1–18.

Cornejo-Garrido, A. G., and P. H. Stone, 1977: On the heat balance of the Walker Circulation. *J. Atmos. Sci.,* **34,** 1155–1162.

Crowley, T. J., 1993: Geological assessment of the greenhouse effect. *Bull. Amer. Meteor. Soc.,* **74,** 2363–2373.

Cunnington, W. M., and J. F. B. Mitchell, 1990: On the dependence of climate sensitivity on convective parameterization. *Climate Dyn.,* **4,** 85–93.

Del Genio, A. D., A. A. Lacis, and R. A. Ruedy, 1991: Simulations of the effect of a warmer climate on atmospheric humidity. *Nature*, **351**, 382–385.

Emanuel, K. A., 1987: The dependence of hurricane intensity on climate. *Nature*, **326**, 483–485.

Goody, R. M., 1964: *Atmospheric Radiation. I. Theoretical Basis.* Oxford University Press, 436 pp.

Gordon, C. T., and W. F. Stern, 1982: A description of the GFDL global spectral model. *Mon. Wea. Rev.*, **110**, 625–644.

Graham, N. E., and T. P. Barnett, 1987: Sea surface temperature, surface wind divergence, and convection over tropical oceans. *Science*, **238**, 657–659.

Guilderson, T. P., R. G. Fairbanks, and J. L. Rubenstone, 1994: Tropical temperature variations since 20,000 years ago: Modulating interhemispheric climate change. *Science*, **263**, 663–665.

Hellerman, S., and M. Rosenstein, 1983: Normal monthly wind stress over the world ocean with error estimates. *J. Phys. Oceanogr.*, **13**, 1093–1104.

Kiehl, J. T., and D. L. Williamson, 1991: Dependence of cloud amount on horizontal resolution in the National Center for Atmospheric Research Community Climate Model. *J. Geophys. Res.*, **96**(D6), 10 955–10 980.

Knutson, T. R., and S. Manabe, 1994: Impact of increased CO_2 on simulated ENSO-like phenomena. *Geophys. Res. Lett.*, **21**, 2295–2298.

Lau, K., C. H. Sui, and W. K. Tao, 1993: A preliminary study of the tropical water cycle and its sensitivity to surface warming. *Bull. Amer. Meteor. Soc.*, **74**, 1313–1321.

Lau, N.-C., S. G. H. Philander, and M. J. Nath, 1992: Simulation of ENSO-like phenomena with a low-resolution coupled GCM of the global ocean and atmosphere. *J. Climate*, **5**, 284–307.

Manabe, S., and A. J. Broccoli, 1985: A comparison of climate model sensitivity with data from the last glacial maximum. *J. Atmos. Sci.*, **42**, 2643–2651.

——, and R. J. Stouffer, 1993: Century-scale effects of increased atmospheric CO_2 on the ocean–atmosphere system. *Nature*, **364**, 215–218.

——, and ——, 1994: Multiple century response of a coupled ocean–atmosphere model to an increase of atmospheric carbon dioxide. *J. Climate*, **7**, 5–28.

——, J. Smagorinsky, and R. F. Strickler, 1965: Simulated climatology of a general circulation model with a hydrologic cycle. *Mon. Wea. Rev.*, **93**, 769–798.

——, K. Bryan, and M. J. Spelman, 1990: Transient response of a global ocean–atmosphere model to a doubling of atmospheric carbon dioxide. *J. Phys. Oceanogr.*, **20**, 722–749.

——, R. J. Stouffer, M. J. Spelman, and K. Bryan, 1991: Transient response of a coupled ocean–atmosphere model to gradual

changes of atmospheric CO_2. Part I: Annual mean response. *J. Climate*, **4**, 785–818.

Meehl, G. A., and W. M. Washington, 1989: Climate sensitivity due to increased CO_2: Experiments with a coupled atmosphere and ocean general circulation model. *Climate Dyn.*, **4**, 1–38.

Mitchell, J. F. B., and W. J. Ingram, 1992: Carbon dioxide and climate: Mechanisms of changes in cloud. *J. Climate*, **5**, 5–21.

——, C. A. Wilson, and W. M. Cunningham, 1987: On CO_2 sensitivity and model dependence of results. *Quart. J. Roy. Meteor. Soc.*, **113**, 293–322.

Neelin, J. D., and I. M. Held, 1987: Modeling tropical convergence based on the moist static energy budget. *Mon. Wea. Rev.*, **115**, 3–12.

Oort, A., 1983: Global atmospheric circulation statistics, 1958–1973, Prof. Paper No. 14. National Oceanic and Atmospheric Administration, 180 pp.

Pan, Y. H., and A. H. Oort, 1983: Global climate variations connected with sea surface temperature anomalies in the eastern equatorial Pacific Ocean for the 1958–73 period. *Mon. Wea. Rev.*, **111**, 1244–1258.

Peixoto, J. P., and A. H. Oort, 1992: *Physics of Climate.* Amer. Inst. Phys., 520 pp.

Philander, S. G. H., R. C. Pacanowski, N.-C. Lau, and M. J. Nath, 1992: Simulation of ENSO with a global atmospheric GCM coupled to a high-resolution, tropical Pacific Ocean GCM. *J. Climate*, **5**, 308–329.

Randall, D. A., et al., 1992: Intercomparison and interpretation of surface energy fluxes in atmospheric general circulation models. *J. Geophys. Res.*, **97**(D4), 3711–3724.

Rasmusson, E. M., and T. H. Carpenter, 1981: Variations in tropical sea surface temperature and surface wind fields associated with the Southern Oscillation/El Niño. *Mon. Wea. Rev.*, **110**, 354–384.

Ropelewski, C. F., and M. S. Halpert, 1987: Global and regional scale precipitation patterns associated with the El Niño/Southern Oscillation. *Mon. Wea. Rev.*, **115**, 1606–1626.

Rosen, R. D., and W. J. Gutowski, 1992: Response of zonal winds and atmospheric angular momentum to a doubling of CO_2. *J. Climate*, **5**, 1391–1404.

Stute, M., M. Forster, H. Frischkorn, J. F. Clark, and P. Schlosser, 1994: A continental paleotemperature record from equatorial Brazil derived from noble gases dissolved in groundwater. *Eos Suppl.*, **75**(44), 381.

Walker, J. C. G., and J. F. Kasting, 1992: Effect of fuel and forest conservation on future levels of atmospheric carbon dioxide. *Paleooceanogr., Paleoclimatol., Paleoecol.*, **97**, 151–189.

Wetherald, R. T., and S. Manabe, 1988: Cloud feedback processes in a general circulation model. *J. Atmos. Sci.*, **45**, 1397–1415.